

Sedimentation and growth of volcanic aerosols within the Hunga plume: Insights from unique tropical in situ and satellite measurements

Giovanni Souza¹, Jean-Paul Vernier², Demilson Quintão³, Bruno Biazon³, Fabio Lopes⁴, Jhonatha Ricardo¹, Amit Kumar Pandit⁵, Rubel Chandra Das⁵, Hongyu Liu⁶, Travis N. N. Knepp⁷, Hazel Vernier⁸, and Eduardo Landulfo⁹

¹Instituto de Pesquisas Energeticas e Nucleares

²Science Systems and Applications, Inc.

³Fundacao para o Desenvolvimento da UNESP

⁴Universidade Federal de Sao Paulo

⁵National Institute of Aerospace

⁶National Institute of Aerospace (NIA) Resident at: NASA Langley Research Center

⁷Nasa Langley

⁸CNRS

⁹Instituto de Pesquisas Energéticas e Nucleares

March 19, 2025

Abstract

The Hunga eruption was an unprecedented event which influenced stratospheric aerosols. This study analyzes the unique dynamics of aerosol plumes using balloon measurements from the Brazil Volcano campaign in Bauru (22.36° S, 49.03° W) and the Stratospheric Aerosol and Gas Experiment III/ISS along with theoretical calculations. They revealed consistent trends in particle sedimentation and spreading. Temporal analysis showed that smaller particles (<225 nm) experienced slower sedimentation rates, with a larger influence by the Brewer-Dobson circulation. Larger particles (>400 nm) exhibited faster sedimentation, descending approximately 3 km by the end of 2022. The descent of the plume into the Upper Troposphere and Lower Stratosphere (UTLS) by February-March 2023 is accompanied by an increase of effective radius from 400 nm to 450 nm due to hygroscopic growth from moist convection. These unique observations suggest that Hunga could have impacted cirrus cloud formation by re-entering the UTLS.

Hosted file

Paper_sedimentation-3-8-2025-Vfinal.docx available at <https://authorea.com/users/901144/articles/1276424-sedimentation-and-growth-of-volcanic-aerosols-within-the-hunga-plume-insights-from-unique-tropical-in-situ-and-satellite-measurements>

Hosted file

Paper_sedimentation-suppl-Mat.docx available at <https://authorea.com/users/901144/articles/1276424-sedimentation-and-growth-of-volcanic-aerosols-within-the-hunga-plume-insights-from-unique-tropical-in-situ-and-satellite-measurements>

Sedimentation and growth of volcanic aerosols within the Hunga plume: Insights from unique tropical in situ and satellite measurements

Giovanni Souza¹, Jean-Paul Vernier^{2,3}, Demilson Quintão⁴, Bruno Biazon⁴, Fábio J. S. Lopes⁵, Jhonatha Ricardo¹, Amit Kumar Pandit², Rubel Chandra Das², Hongyu Liu³, Travis Knepp³, Hazel Vernier^{6,7}, Eduardo Landulfo¹

¹Instituto de Pesquisas Energéticas e Nucleares IPEN-CNEN, São Paulo, SP, Brasil.

²National Institute of Aerospace, Hampton, VA, USA

³NASA Langley Research Center, Hampton, VA, USA

⁴Centro de Meteorologia de Bauru IPMet-UNESP, Bauru, SP, Brasil

⁵Instituto de Ciências Ambientais, Químicas e Farmacêuticas - ICAQF/UNIFESP, São Paulo, SP, Brasil.

⁶University of Reims, Champagne-Ardenne, GSMA, CNRS, UMR 7331-France

⁷Laboratoire de Physique et Chimie de l'Environnement et de l'Espace, (LPC2E), CNRS, Université d'Orléans- France

Key points

- Unique combination of in situ and satellite measurements to study Hunga plume microphysics
- Vertical evolution and spread explained by sedimentation and Brewer-Dobson circulation
- Evidence for aerosol growth near the tropopause and potential impact on cirrus cloud

Abstract

The Hunga eruption was an unprecedented event which influenced stratospheric aerosols. This study analyzes the unique dynamics of aerosol plumes using balloon measurements from the Brazil Volcano campaign in Bauru (22.36° S, 49.03 °W) and the Stratospheric Aerosol and Gas Experiment III/ISS along with theoretical calculations. They revealed consistent trends in particle sedimentation and spreading. Temporal analysis showed that smaller particles (<225 nm) experienced slower sedimentation rates, with a larger influence by the Brewer-Dobson circulation. Larger particles (>400 nm) exhibited faster sedimentation, descending approximately 3 km by the end of 2022. The descent of the plume into the Upper Troposphere and Lower Stratosphere (UTLS) by February-March 2023 is accompanied by an increase of effective radius from 400 nm to 450 nm due to hygroscopic growth from moist convection. These unique observations suggest that Hunga could have impacted cirrus cloud formation by re-entering the UTLS.

40 Plain Language Summary

41 The Hunga eruption was an unprecedented event which influenced stratospheric
42 aerosols. This study analyzes balloon measurements from the Brazil Volcano campaign in
43 Bauru (22.36° S, 49.03 °W) and remote sensing satellite observations along with theoretical
44 calculations. We show that the vertical evolution of the aerosol plume is consistent with particle
45 settling and the general stratospheric circulation. Temporal analysis showed that smaller
46 particles are less affected by sedimentation and subject to uplift by vertical motion compared to
47 large particles. The descent of the plume near the tropopause by February-March 2023 is
48 accompanied by an aerosol growth due to increase of moisture. These unique observations
49 suggest that Hunga could have impacted the formation of cirrus clouds near the tropopause.

50 1. Introduction

51
52 Stratospheric aerosols play a critical role in the Earth's climate, atmospheric chemistry
53 and dynamics (Kremser et al. 2016). On January 15th, 2022, the eruption of the Hunga Tonga-
54 Hunga Ha'apai (Hunga) injected a modest 0.42 Tg of SO₂ but reached mesospheric levels near
55 57 km (Proud et al., 2022; Carr et al., 2022). Additionally, this eruption injected approximately
56 150 Tg of water vapor into the stratosphere, which represents almost 10% of the global water
57 vapor presence in the stratosphere (Millán et al., 2022; Zhu et al., 2022). The Hunga eruption
58 produced a global Stratospheric Aerosol Optical Depth (SAOD) near ~0.016 close to the SAOD
59 peak after the Raikoke eruption. However, the Raikoke event injected thrice the amount of SO₂
60 (Carn et al., 2022). The higher extinction efficiency of sulfate aerosol produced through
61 coagulation due to the large water vapor injected and the longer residence time may explain this
62 unusual SAOD (Asher et al., 2023). Initial SO₂ estimates might be largely underestimated (Carn
63 et al. 2022, Hunga workshop Paris), given the rapid production of sulfate in the fresh plume
64 which would have resulted in the rapid conversion of SO₂. Finally, the marine water injection
65 (Khaykin et al., 2022) evident of HDO/H₂O isotopic ratio (δD) by from ACE-FTS observations
66 could have also led to the injection of marine aerosols.

67 Ground-based observations from the AERosol RObotic NETwork (AERONET, Holben et
68 al., 1998) have shown that sulfate aerosols have experienced rapid growth to 300-500 nm
69 particle diameters (Boichu et al., 2023). The increase in aerosol optical depth monitored from in
70 situ and satellite observations was one of the most significant ever since the 1991 Mt. Pinatubo
71 eruption (Asher et al., 2023).

72 Limited balloon-borne measurements of aerosol plumes provided insights into the
73 microphysical, spatial, and temporal variations within the Hunga plume (Asher et al., 2023;
74 Kloss et al., 2022; Deshler et al., 2024; Bian et al., 2023). These measurements indicate that
75 the Hunga impact produced particles larger than 500 nm in diameter several months after the
76 eruption (Deshler et al. 2024; Bian et al. 2023). Asher et al. (2023) underscored the rapid
77 formation of aerosols following the Hunga Tonga eruption facilitated by the humidification of the

78 stratosphere. This increased humidity led to rapid and substantial ozone depletion likely from
79 heterogeneous ozone chemistry due to injected sea salt (Evan et al., 2023; Zhu et al., 2023).

80 A comprehensive analysis (Li et al., 2024) of the microphysical processes in the Hunga
81 plume between 0 and 30°S using the CESMI-CERMA aerosol model showed that the aerosol
82 effective radius grew to peak at 400 nm in the early plume. The water vapor injected likely
83 favored the coagulation growth by increasing the oxidation rate of SO₂, which led to an increase
84 in the concentration of small particles that coagulated (Li et al. 2024). After 4 months, this study
85 showed that the average effective radius between 20 and 25 km decreased due to
86 sedimentation of large particles. The apparent sedimentation and growth of large particles near
87 the tropopause was observed by SAGE III/ISS in February and March 2023 more than one year
88 after the eruption (Knepp et al. 2024).

89 However, significant gaps remain in our understanding, due to the lack of continuous in-
90 situ measurements in the tropics, which limits our ability to study the long-term evolution and
91 behavior of the plume. Here we investigate the mechanisms responsible for the vertical
92 evolution of Hunga plume and separate the effect of dynamics, sedimentation, and aerosol
93 growth. We combine for the first time aerosol size distribution from balloon measurements
94 conducted in Brazil and Particle Size Distribution (PSD) product from the Stratospheric Aerosol
95 and Gas Experiment (SAGE) III/ISS.

96 The focus of this work is to: 1 - derive microphysical properties of the Hunga plume
97 using optical particle counters; 2 - compare and associate OPC measurements with those from
98 SAGE III/ISS observations; 3 - separate the role of sedimentation and dynamics in the vertical
99 evolution of the Hunga plume; 4 - Estimate the hygroscopic growth of volcanic aerosols
100 observed near the tropopause.

101

102 **2. Methodology**

103

104 **2.1. BraVo Campaign**

105

106 This study utilizes data collected during the Brazil Volcano project (BraVo) campaign,
107 conducted at the Centro de Meteorologia de Bauru (IPMET-UNESP) in Bauru, Brazil (-22.28, -49.25),
108 from May 24th, 2022, to August 13th, 2023. Thirteen balloon flights were carried out, deploying a
109 suite of instruments including a Profiling Optical Counter (POPC), Compact Backscatter Aerosol
110 Detector (COBALD), Cryogenic Frost Point Hygrometer (CFH), Electro-Chemical Counter (ECC), and
111 an Aerosol Sampler. The POPC, which measures aerosol size distribution and concentration, is
112 central to this analysis, providing crucial information for investigating sedimentation and aerosol
113 growth processes within the plume. To complement the in-situ POPC measurements, we incorporate
114 PSD product from SAGE III/ISS.

115

116 **2.2. POPC**

117

118 We employed the Profiling Optical Particle Counter (POPC, Dumelie et al., 2024; Li et
119 al., 2023). Its sensitivity ranges from 0.3 μm to 10 μm with 30 particle diameter channels. The

120 calibration of the instrument is done with Polyethylene Spherical Particles (PSL). Since the
121 scattering efficiency of PSL is higher than sulfate or sea salt aerosol, we applied a correction
122 factor on the size threshold of the POPC data (see Figure S1).

123 The first balloon was launched 4 months after the eruption, 12 POPC occurred in total
124 during 19 months with two intensive campaigns in May and August 2022. The balloon ascended
125 to the stratosphere and burst at an altitude between 26 to 32 km above sea level, capturing the
126 vertical extent of the plume. The system collects data at a 0.5 Hz frequency. POPC was used to
127 study volcanic plumes after several volcanic eruptions (Li et al. 2023; Dumelié et al. 2024). It
128 compared well with other counters such as Printed Optical Particle Spectrometer (POPS) and
129 stratospheric aerosol extinction measurements from SAGE III/ISS.

130 This study provides multiple observations of the Hunga plume to investigate its vertical
131 displacement and separate the contributions of the sedimentation, dynamics, and aerosol
132 growth.

133
134

135 **2.3. SAGE III/ISS**

136

137 The Stratospheric Aerosol and Gas Experiment III (SAGE III/ISS), mounted on the
138 International Space Station (ISS) (Cisewski, et al., 2014), was utilized to analyze the
139 stratospheric aerosol properties following the Hunga eruption (Knepp et al., 2024). SAGE III/ISS
140 operates by scanning the limb of the Earth's atmosphere during solar and lunar occultations,
141 offering a unique advantage point from the ISS's orbit. This method provides highly accurate
142 vertical profiles of aerosols and gases by measuring the attenuation of solar or lunar light as it
143 passes through the atmosphere (Chu et al., 1999).

144 We use profiles of the extinction coefficient (Level 2, v5.2) at 1020 nm, water vapor
145 mixing ratio and the PSD product (Knepp et al., 2024) from the SAGE III/ISS data. The PSD
146 product (V1.1) includes the “Number Density”, “Mode Radius”, “Standard Deviation”, and their
147 associated uncertainty. It is based on finding the best solutions for number density, mode
148 radius, and sigma to reproduce aerosol extinction spectra using Mie theory calculation. SAGE
149 III/ISS PSD product variables are used to derive POPC-like observations (number concentration
150 above the 30 sizes threshold).

151 The data collection was specifically timed to capture the dispersion of the volcanic plume
152 as the ISS orbited over Bauru with the co-location criteria of +/- 10 degrees in longitude and
153 latitude. During the campaign, three balloon flights were collocated with SAGE III/ISS
154 observations within 100 hours of separation from the balloon measurements (see table S1
155 supplementary materials).

156
157
158
159
160
161
162
163

164

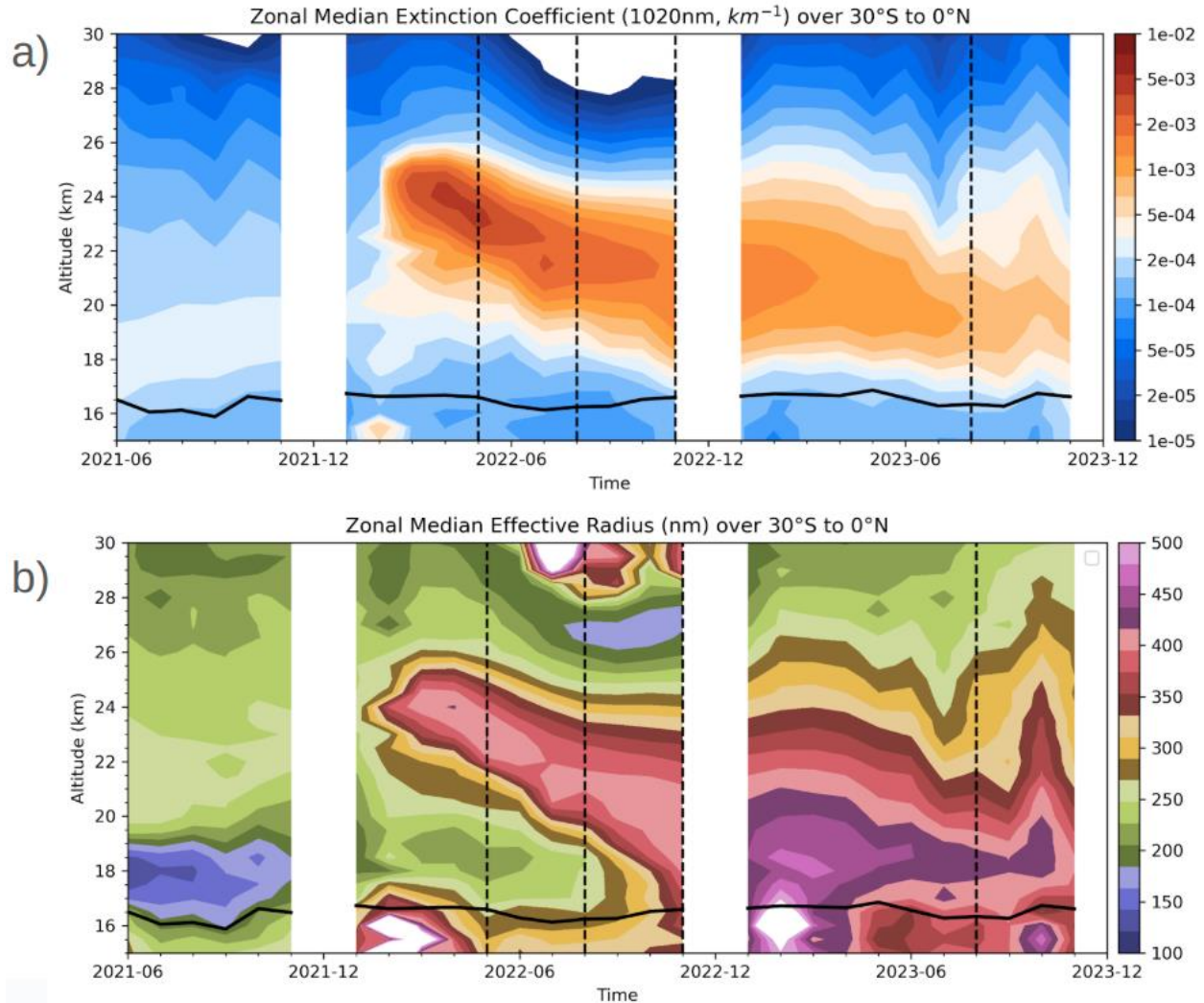
165 **3. Results**

166

167 **3.1. Observational evidence for the vertical displacement of** 168 **the Hunga Plume**

169

170 The Hunga aerosol plume was observed up to ~40 km with OMPS-LP (Taha et al., 2022) and
171 CALIOP (Sellito et al., 2022) within a few days after the eruption. Within 3 weeks, the plume
172 descended to 24-26 km likely due to the radiative cooling from water vapor (Sellito et al., 2022;
173 Legras et al., 2022). Figure 1 shows the zonal median aerosol extinction coefficient at 1020 nm
174 and effective radius profiles from SAGE III/ISS between 0-30 °S from June 2021 to November
175 2023. The aerosol plume is observed with a maximum extinction coefficient at 1020 nm,
176 descending from 25 km in January 2022 to near the tropopause at 16.5 km by November 2022.
177 During the descent, the plume width increased by several kilometers, likely affected by both
178 sedimentation and vertical uplift of the Brewer-Dobson circulation. This is a unique behavior for
179 a volcanic plume in the tropics for the past 2 decades. The zonal mean scattering ratio profiles
180 in Figure S1 show that all the plumes observed by CALIOP ascended in the stratosphere due to
181 the upper branch of the Brewer-Dobson circulation (Vernier et al., 2009; Fairlie et al., 2014) but
182 the Hunga plume had a different behavior. Knepp et al. (2024) proposed that the sedimentation
183 was mostly responsible for the descent and vertical spread of the plume in the tropics. Another
184 very interesting feature in Figure 2 is the aerosol growth from an effective radius of 400 nm in
185 August 2022 to nearly 450 nm in February-March 2023 between 18-20 km. While Knepp et al.
186 (2024) identified these features, this study delves deeper into the mechanisms driving the
187 plume's vertical displacement. Specifically, we investigate the roles of sedimentation, the
188 dynamics, and hygroscopic growth, aspects not addressed in previous work. We combined in
189 situ measurements with SAGE III/ISS to further study the plume's microphysical evolution.



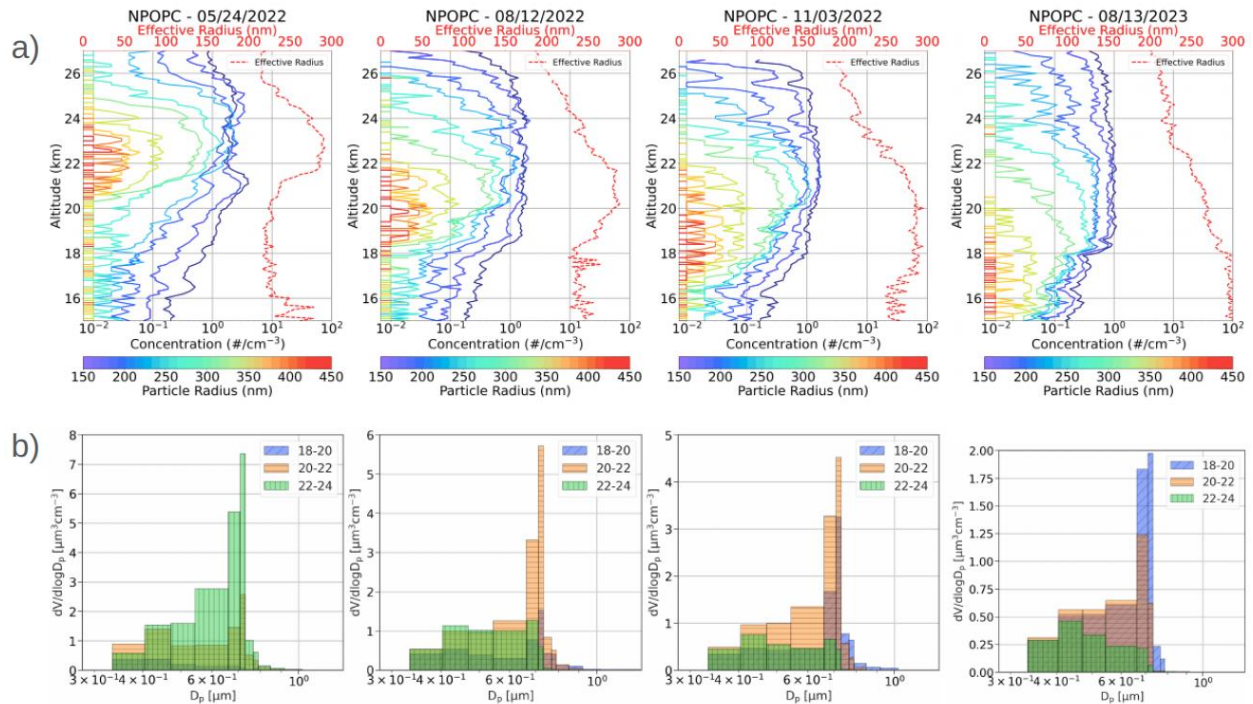
190
 191 **Figure 1.** - (a) Monthly zonal median profile evolution between 0-30°S of aerosol extinction at
 192 1020 nm and effective radius. (b) from SAGE III/ISS from June 2021 to November 2023. The
 193 vertical dashed lines show the measurement periods of the BraVo campaigns in May 2022,
 194 August 2022, November 2023, and August 2023. The tropopause level is shown by the solid
 195 black line.

196 Figure 2 shows POPC differential concentration profiles and effective radius to track the
 197 evolution of the Hunga plume. The concentration profiles across ten different particle sizes are
 198 displayed in the upper panel of Figure 2. The maximum concentrations, which occur at varying
 199 altitudes depending on the date, decrease as the plume descends over time, indicating gradual
 200 sedimentation. For instance, on May 24th, 2022, the highest concentration is observed around
 201 21 km with values of 3 $\#/cm^3$ for particles near 200 nm while the peak for those near 300 nm
 202 was approximately 0.5 $\#/cm^3$ near 23 km. The concentration values decrease in subsequent
 203 profiles, reflecting the plume's descent through the stratosphere and the diffusion of the plume
 204 through its transport in the southern hemisphere mid-latitudes. Measurements made on
 205 November 3rd, 2022, showed that the total number for $r>250$ nm peaked near 1-2 $\#/cm^3$, a
 206 value close to the one reported by Deshler et al. (2024) at 12 km over McMurdo station in

207 Antarctica a few months later in April 2023. The effective radius (r_{eff}) peaked near 21.5-24 km
208 on May 24th, 2022, near 290 nm, progressively descending to 20-22 km on August 12th, 2022,
209 spreading between 17-22 km by November 3rd, 2022. The r_{eff} maximum continues spreading
210 to levels below the tropopause by August 2023. r_{eff} maximum increased from 290 nm to 300
211 nm from May 2022 to August 2023. Relative to SAGE III/ISS, the peak r_{eff} observed by the
212 POPC is lower by ~30% but still in the lower range of estimates from Boone et al. (2024) who
213 found a r_{eff} between 280-400 nm. POPC counting efficiency near 50% for $r > 150$ nm may also
214 explain some of the discrepancies with SAGE III/ISS. Around 5 months after the eruption, Li et
215 al. (2024) reported POPS measurement near Reunion Island [21S, 55.4E] located at a similar
216 latitude as Bauru. They showed mean r_{eff} between 20-25 km around 330 nm, as well as profiles
217 with a peak near 430 nm on March 31st, 2022, consistent with SAGE III/ISS.

218 The lower panels of Figure 2 present histograms of particle size distributions at three
219 distinct altitude ranges (18-20 km, 20-22 km, and 22-24 km), showing a shift towards larger
220 particle sizes at lower altitudes. This trend is particularly evident in the progressive increase in
221 the volume of larger particles, especially in the 500 to 1000 nm range, as shown in the
222 histograms from higher to lower altitude bands.

223 SAGE III/ISS shows that the main plume contained particles with effective radii greater
224 than 400 nm, and over time a partitioning between larger particles (> 400 nm) and smaller
225 particles (< 300 nm) was observed, with the largest particles showing a rapid descent compared
226 to the smaller ones (Knepp et al., 2024). By March/June 2023, some particles approached 500
227 nm near 18 km indicating significant growth and sedimentation over the period. This is
228 consistent with observations from Boichu et al. (2023) who observed through column integrated
229 AERONET data a peak radius progressively increasing from July 2022 to January 2023 near
230 500 nm. Further theoretical considerations are provided here to interpret these observations.



231
 232 Figure 2 - The upper panels show the particle concentration profiles from POPC for 10 size
 233 ranges between 150 and 450 nm, different sizes are represented by the colors. The lower
 234 panels show the distribution of particle diameter for three different altitude ranges.

235
 236

237 3.2. Sedimentation and dynamical processes responsible for 238 the vertical evolution of the Hunga plume

239

240 We derived further parameters and chose the lognormal fit of the concentration profiles
 241 to provide both the maximum and width of the plume (supp. mat.). Repeating the process for all
 242 POPC data collected, we derived the temporal evolution of these quantities. We collocated 3
 243 balloon flights with SAGE III/ISS overpasses during the BraVo campaign. For comparisons with
 244 POPC, the 3 parameters of the lognormal distribution (mode radius, standard deviation, total
 245 concentration) from the SAGE III/ISS PSD product were used to obtain the concentration above
 246 a size threshold to mimic and fill the gaps in the POPC measurements. Fitted concentration
 247 profiles for $r > 150$ nm between are shown in Figure 3b, where we can see that SAGE III/ISS
 248 underestimate the concentration compared to POPC by about 40%. However, the altitude of
 249 detection of the plume is consistent between the two instruments. Figure 3a shows the evolution
 250 of the plume with both SAGE III and POPC data merged. Both instruments show the descent
 251 of the plume by ~ 3 km from January 2022 to August 2022 before reaching a plateau until May 2023
 252 and descend again afterward. The larger aerosols ($r > 300$ nm) appear to descend faster than the
 253 smaller sizes. SAGE III/ISS PSD product shows the same sedimentation behavior in the first
 254 months after the eruption and also shows that the plume started to rise around October 2022,
 255 keeping a roughly constant altitude before descending again.

256 We used sedimentation calculations along with zonal mean vertical wind from MERRA-2
257 to try to reproduce these observations.

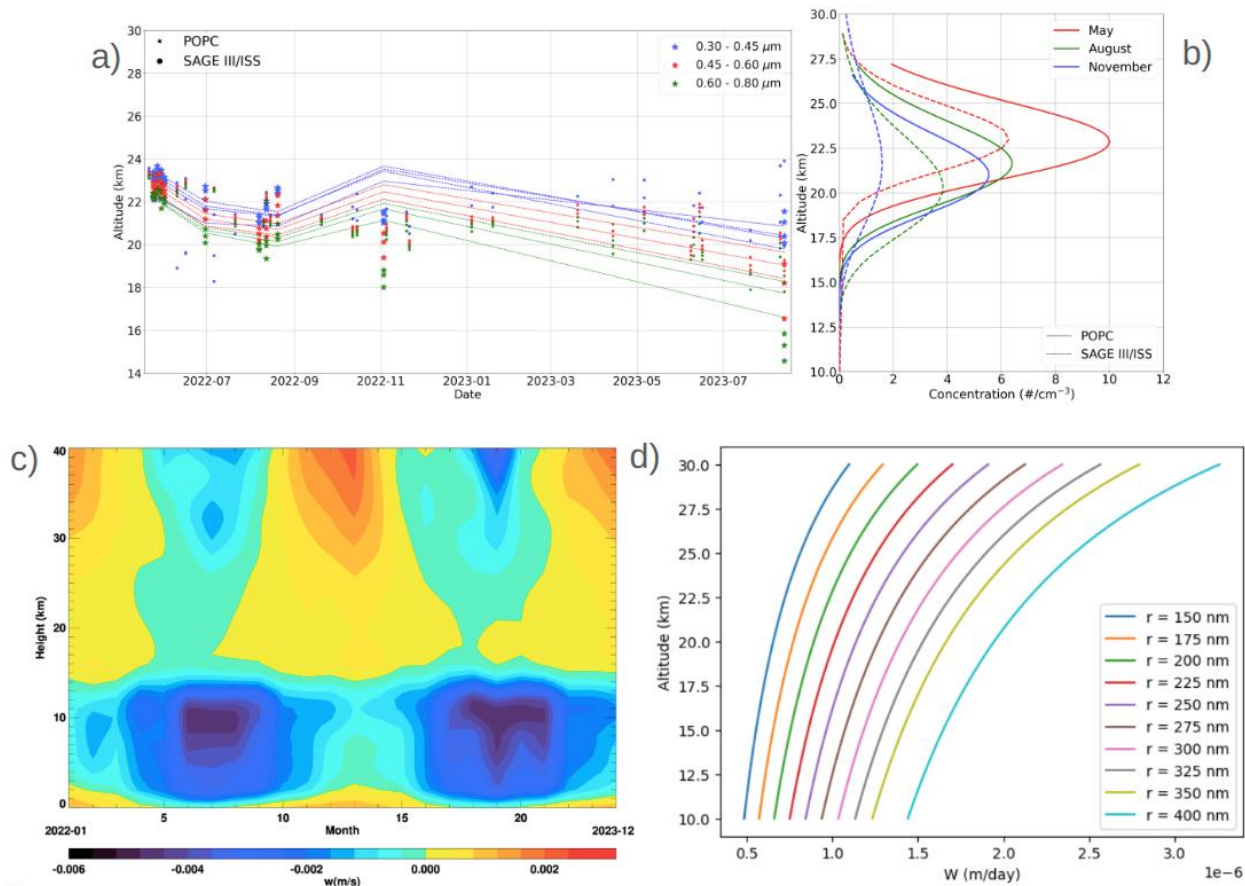
258
259 We apply Stokes' Law to estimate their settling velocity (W) under laminar flow
260 conditions:

$$261 \quad W = \frac{C\rho_p r^2 g}{18\eta} \quad (1)$$

262 where g is the acceleration due to gravity, r is the radius of the particle, ρ is the particle
263 density, and η is the viscosity of air. C is written as environmental factors (e.g. temperature,
264 pressure, and humidity) that can affect these variables, requiring adjustments to the calculation,
265 especially for non-spherical particles or in turbulent flow conditions. Figure 3d shows the
266 sedimentation for several values of radius in the same range as POPC channels.

267 The other factor affecting the plume's vertical evolution is the dynamics of the
268 stratosphere and updraft from the tropical branch of the Brewer-Dobson circulation in the
269 tropics. The vertical wind was calculated using MERRA-2 reanalysis dataset, which calculates
270 vertical wind speeds by integrating observations with model forecasts, adjusting through
271 physical laws and continuity equations, and ensuring consistency with observed atmospheric
272 conditions (Gelaro et al., 2017). Figure 3c shows that the vertical wind was near 0 during the
273 first part of the BraVo campaign in May 2022 becoming positive after August.

274 The theoretical calculations match the initial plume motion. However, the theoretical
275 plume rise was 2 km higher than observed in November 2022. On the other hand, after May
276 2023, the plume altitude was underestimated compared to SAGE III/ISS. The particles show
277 similar behavior with time, comparing the initial and final launch. The smaller particles seem to
278 have slower sedimentation rate compared to the large ones, as expected from theory. However,
279 the plume shows a different behavior in August 2023 compared with the theoretical curve. The
280 plume rises above the predicted curve, indicating a more complex dynamics, reflecting some
281 inhomogeneity in the plume dispersion.



282 Figure 3. (a) The maximum of the lognormal fit corresponding to each size range shown by
 283 blue, red and green colored stars (for POPC) and dots (for SAGE III/ISS). Dotted lines represent
 284 the theoretical sedimentation velocity estimated for each POPC measurement. (b) Profiles of
 285 particle concentration for POPC and SAGE III/ISS during May (red), August (green) and
 286 November (blue) of 2022. (c) Zonally averaged (between 20°S - 30°S) vertical velocity derived
 287 from MERRA-2 reanalysis. (d) Sedimentation velocity for particles at different POPC size
 288 (radius) channels.
 289

290
 291

292 3.3. Hygroscopic Growth of Hunga Aerosols

293

294 After more than one year from the Hunga eruption, the sedimentation and transport of the
 295 volcanic plume lead to changes in its microphysical properties. The zonal mean r_{eff} from SAGE
 296 III/ISS illustrated in Figure 1 shows that the plume descended more than 5km, from January
 297 2022 to March 2023, and increased from ~ 400 nm at 24-26 km to 450 nm near 18 km. This
 298 indicates that aerosol within the plume underwent growth while reaching tropopause levels. The
 299 mechanism behind this growth is probably the increase in the relative humidity (RH) at lower
 300 altitudes, which might have favored the condensation of water droplets on volcanic aerosols.
 301 Figure 4a shows the zonal (0-30° S) mean RH profile from June 2021 to November 2023
 302 derived from SAGE III/ISS water vapor mixing ratio and temperature from MERRA-2 (see
 303 method in supp. mat.). We overplotted on the RH contour the r_{eff} . At 18 km, the RH shows a

304 significant seasonal variation with maxima between January and March during the convective
 305 periods in the Southern hemisphere. During the descent, the RH within the plume goes from 2%
 306 to more than 40% which coincides with the increase in the r_{eff} . To model the particle growth, we
 307 took an effective radius (r_{eff}) profile from August 2022 and compared it with a profile on March
 308 2023 in Figure 4b. We used hygroscopic growth with kappa-Köhler (Titos et al., 2016) theory
 309 that can be written as follows:

$$310 \quad GF(RH) = \frac{r_{wet}}{r_{dry}} = \left(1 + K \times \frac{RH}{100 - RH} \right)^{1/3} \quad (2)$$

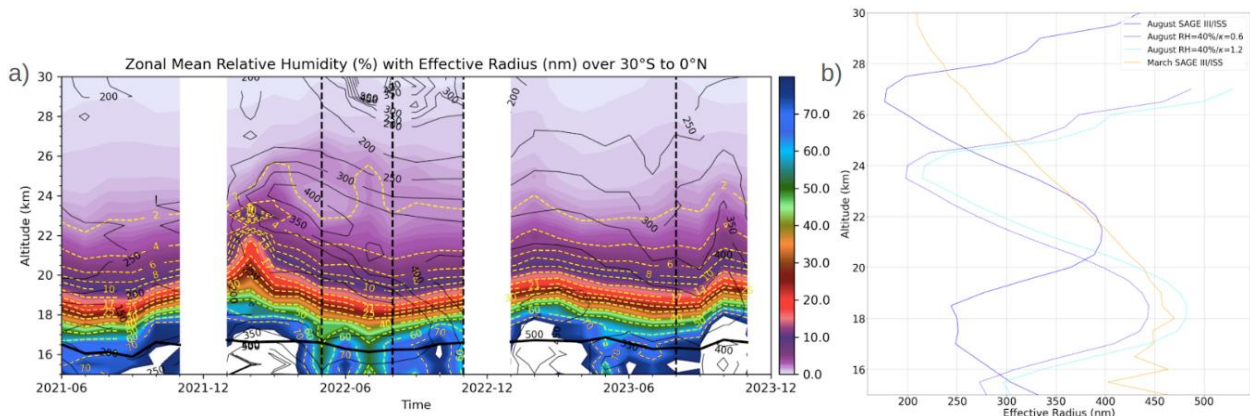
311
 312 Where:

- 313 • r_{wet} is the wet diameter of the aerosol particle.
- 314 • r_{dry} is the dry diameter of the aerosol particle.
- 315 • K is the hygroscopicity parameter known as Kappa
- 316 • RH is the relative humidity expressed as %

317 Using equation (2), we can show that growth factor (GF) can be expressed for hygroscopic
 318 growth from RH1 to RH2 by:

$$319 \quad GF(RH_1, RH_2, K) = \left(\frac{100 - RH_1}{100 - RH_2} \times \frac{100 - RH_2(1 - K)}{100 - RH_1(1 - K)} \right)^{1/3} \quad (3)$$

320 Applying the theory to the profile in August 2022, assuming the presence of ammonium sulfate
 321 particles (Kappa=0.6) and an increase in the RH of 40%, we see that the r_{eff} almost matches the
 322 values observed in March 2023. The corresponding growth assuming the presence of sea salts
 323 (Kappa=1.2) produces values above 450 nm. These calculations seem to indicate that the
 324 aerosol plume growth can be explained by hygroscopic processes.



325
 326

327 Figure 4. (a)- Filled color contours show the time-series (June 2021 - November 2023) of zonal
328 mean relative humidity between 15 and 30 km altitude averaged over 0 - 30° S. Relative
329 humidity is derived from SAGE III/ISS water vapor mixing ratio and MERRA-2 temperature
330 profiles using Murphy and Koop (2005). Black contour lines superimposed on the color contour
331 show the effective radius obtained from the SAGE III/ISS PSD product. (b) Comparison
332 between August 2022 and March 2023 r_{eff} profiles from SAGE III/ISS.
333

334 4. Conclusion

335

336 This study investigated the dynamics of aerosol plumes from the Hunga eruption using
337 in-situ measurements and satellite observations from SAGE III/ISS during the BraVo campaign
338 in 2022 and 2023. By applying lognormal fits to the aerosol concentration profiles, we derived
339 key parameters such as plume width and center altitude, revealing insights into the plume's
340 evolution.

341 The BraVo campaign included three balloon flights coordinated with the ISS passages,
342 enabling a unique comparison between POPC and SAGE III/ISS observations. Both instruments
343 detected the plume at similar altitudes, with SAGE III/ISS corroborating the POPC's findings of
344 sedimentation and plume dispersion. However, the POPC recorded 40% - 50% higher
345 concentrations than SAGE III/ISS within the plume (Figure 3), possibly due to differences in
346 instrument sensitivities or measurement techniques.

347 Our analysis revealed distinct temporal changes in plume behavior. Smaller particles (<
348 250 nm) exhibited slower sedimentation and greater vertical spreading compared to larger
349 particles. These smaller particles gradually descended by ~2 km before being lifted again by the
350 Brewer-Dobson circulation, returning to their initial altitudes by late 2022. Conversely, larger
351 particles (225-400 nm) experienced faster sedimentation, moderated by the Brewer-Dobson
352 circulation, resulting in a ~3 km descent by late 2022.

353 Plume width also varied with particle size. Smaller particles showed limited lateral
354 spreading, while larger particles, especially those > 300 nm, exhibited an increase in plume
355 width of over 2 km.

356 Using equations for sedimentation and vertical wind from MERRA-2, the vertical
357 displacement of the particles during the first one and a half year after the eruption was
358 reproduced. Aerosol growth observed near 18 km observed from February to March 2023 can
359 be explained by the increase of relative humidity during the convective season, which led to
360 hygroscopic growth. This indicates that the sedimenting Hunga plume might have influenced the
361 formation of cirrus clouds near the tropopause during that time, but this needs further
362 investigation.

363

364 Acknowledgments

365

366 This research was funded by the Brazil Research fundation (CAPES) (Scholarship:
367 88887.859244/2023-00). We acknowledge the NASA Upper Atmospheric Composition
368 Observation program and the Stratospheric Aerosol and Gas Experiments (UACO, SAGE) for

369 their supports. Additional support was provided by the Agence Nationale de la Recherche
370 (ANR) through grant ANR-LABX-100-01 from Labex VOLTAIRE, managed by the University of
371 Orleans.

372 We thank Johnny Mau for his technical assistance in preparing the balloon campaign.
373

374 **Open Research**

375
376 The SAGE data are available at <https://asdc.larc.nasa.gov/project/SAGE%20III-ISS>. We used
377 Python codes available online.
378

379 **References**

380
381 Asher, E., Todt, M., Rosenlof, K., Thornberry, T., Gao, R.-S., Taha, G., et al. (2023).
382 Unexpectedly rapid aerosol formation in the Hunga Tonga plume. *Proceedings of the National*
383 *Academy of Sciences*, 120(46). <https://doi.org/10.1073/pnas.2219547120>

384
385 Benoit, R., Vernier, H., Vernier, J.-P., Joly, L., Dumelié, N., Wienhold, F. G., et al. (2023). The
386 first balloon-borne sample analysis of atmospheric carbonaceous components reveals new
387 insights into formation processes. *Chemosphere*, 326, 138421.
388 <https://doi.org/10.1016/j.chemosphere.2023.138421>
389

390
391 Bian, J., Li, D., Bai, Z., Xu, J., Li, Q., Wang, H., et al. (2023). First detection of aerosols of the
392 Hunga Tonga eruption in the Northern Hemisphere stratospheric westerlies. *Science Bulletin*,
393 68(6), 574–577. <https://doi.org/10.1016/j.scib.2023.03.002>

394
395 Boichu, M., Grandin, R., Blarel, L., Torres, B., Derimian, Y., Goloub, P., et al. (2023). Growth
396 and global persistence of stratospheric sulfate aerosols from the 2022 Hunga Tonga–Hunga
397 Ha’apai volcanic eruption. *Journal of Geophysical Research Atmospheres*, 128(23).
398 <https://doi.org/10.1029/2023jd039010>

399
400 Boone, C. D., Bernath, P. F., Pastorek, A., & Lecours, M. (2023). Sulfate aerosol properties
401 derived from combining coincident ACE-FTS and SAGE III/ISS measurements. *Journal of*
402 *Quantitative Spectroscopy and Radiative Transfer*, 312, 108815.
403 <https://doi.org/10.1016/j.jqsrt.2023.108815>

404
405 Carn, S. A., Krotkov, N. A., Fisher, B. L., & Li, C. (2022). Out of the blue: Volcanic SO₂
406 emissions during the 2021–2022 eruptions of Hunga Tonga—Hunga Ha’apai (Tonga). *Frontiers*
407 *in Earth Science*, 10. <https://doi.org/10.3389/feart.2022.976962>

408
409 Carr, J. L., Horváth, Á., Wu, D. L., & Friberg, M. D. (2022). Stereo plume height and motion
410 retrievals for the Record-Setting Hunga Tonga–Hunga Ha’apai eruption of 15 January 2022.
411 *Geophysical Research Letters*, 49(9). <https://doi.org/10.1029/2022gl098131>

412 Cisewski, M., Zawodny, J., Gasbarre, J., Eckman, R., Topiwala, N., Rodriguez-Alvarez, O., et
413 al. (2014). The Stratospheric Aerosol and Gas Experiment (SAGE III) on the International Space
414 Station (ISS) mission. *Proceedings of SPIE, the International Society for Optical*
415 *Engineering/Proceedings of SPIE*, 9241, 924107. <https://doi.org/10.1117/12.2073131>
416

417 Deshler, T., Kalnajs, L. E., Norgren, M., Zhu, Y., & Zhang, J. (2024). In situ aerosol size spectra
418 measurements in the Austral polar vortex before and after the Hunga Tonga-Hunga Ha'apai
419 volcanic eruption. *Geophysical Research Letters*, 51(22). <https://doi.org/10.1029/2024gl111388>
420

421 Dumelié, N., Vernier, J. -p., Berthet, G., Vernier, H., Renard, J. -b., Rastogi, N., et al. (2023).
422 Toward rapid balloon experiments for sudden aerosol injection in the stratosphere (REAS) by
423 volcanic eruptions and wildfires. *Bulletin of the American Meteorological Society*, 105(1), E105–
424 E120. <https://doi.org/10.1175/bams-d-22-0086.1>
425

426 Evan, S., Brioude, J., Rosenlof, K. H., Gao, R.-S., Portmann, R. W., Zhu, Y., et al. (2023). Rapid
427 ozone depletion after humidification of the stratosphere by the Hunga Tonga Eruption. *Science*,
428 382(6668). <https://doi.org/10.1126/science.adg2551>
429

430 Fairlie, T. D., Vernier, J. -p., Natarajan, M., & Bedka, K. M. (2014). Dispersion of the Nabro
431 volcanic plume and its relation to the Asian summer monsoon. *Atmospheric Chemistry and*
432 *Physics*, 14(13), 7045–7057. <https://doi.org/10.5194/acp-14-7045-2014>
433

434 Hagan, D. H., & Kroll, J. H. (2020). Assessing the accuracy of low-cost optical particle sensors
435 using a physics-based approach. *Atmospheric Measurement Techniques*, 13(11), 6343–6355.
436 <https://doi.org/10.5194/amt-13-6343-2020>
437

438 Holben, B. N., Eck, T. F., Slutsker, I., Tanré, D., Buis, J. P., Setzer, A., et al. (1998).
439 AERONET—A federated instrument network and data archive for aerosol characterization.
440 *Remote Sensing of Environment*, 66(1), 1–16. [https://doi.org/10.1016/s0034-4257\(98\)00031-5](https://doi.org/10.1016/s0034-4257(98)00031-5)
441

442 Khaykin, S., Legras, B., Bucci, S., Sellitto, P., Isaksen, L., Tencé, F., et al. (2020). The 2019/20
443 Australian wildfires generated a persistent smoke-charged vortex rising up to 35 km altitude.
444 *Communications Earth & Environment*, 1(1). <https://doi.org/10.1038/s43247-020-00022-5>
445

446 Khaykin, S., Podglajen, A., Ploeger, F., Groß, J.-U., Tence, F., Bekki, S., et al. (2022). Global
447 perturbation of stratospheric water and aerosol burden by Hunga eruption. *Communications*
448 *Earth & Environment*, 3(1). <https://doi.org/10.1038/s43247-022-00652-x>
449

450 Kloss, C., Sellitto, P., Renard, J., Baron, A., Bègue, N., Legras, B., et al. (2022). Aerosol
451 characterization of the stratospheric plume from the volcanic eruption at Hunga Tonga 15
452 January 2022. *Geophysical Research Letters*, 49(16). <https://doi.org/10.1029/2022gl099394>
453

454 Knepp, T. N., Kovilakam, M., Thomason, L., & Miller, S. J. (2024). Characterization of
455 stratospheric particle size distribution uncertainties using SAGE II and SAGE III/ISS extinction

456 spectra. *Atmospheric Measurement Techniques*, 17(7), 2025–2054. <https://doi.org/10.5194/amt->
457 17-2025-2024

458

459 Kremser, S., Thomason, L. W., Von Hobe, M., Hermann, M., Deshler, T., Timmreck, C., et al.
460 (2016). Stratospheric aerosol-Observations, processes, and impact on climate. *Reviews of*
461 *Geophysics*, 54(2), 278–335. <https://doi.org/10.1002/2015rg000511>

462

463 Legras, B., Duchamp, C., Sellitto, P., Podglajen, A., Carboni, E., Siddans, R., et al. (2022). The
464 evolution and dynamics of the Hunga Tonga–Hunga Ha’apai sulfate aerosol plume in the
465 stratosphere. *Atmospheric Chemistry and Physics*, 22(22), 14957–14970.
466 <https://doi.org/10.5194/acp-22-14957-2022>

467

468 Li, C., Peng, Y., Asher, E., Baron, A. A., Todt, M., Thornberry, T. D., et al. (2024). Microphysical
469 simulation of the 2022 Hunga volcano eruption using a sectional aerosol model. *Geophysical*
470 *Research Letters*, 51(11). <https://doi.org/10.1029/2024gl108522>

471

472 Li, Y., Pedersen, C., Dykema, J., Vernier, J.-P., Vattioni, S., Pandit, A. K., et al. (2023). In situ
473 measurements of perturbations to stratospheric aerosol and modeled ozone and radiative
474 impacts following the 2021 La Soufrière eruption. *Atmospheric Chemistry and Physics*, 23(24),
475 15351–15364. <https://doi.org/10.5194/acp-23-15351-2023>

476

477 Millán, L., Santee, M. L., Lambert, A., Livesey, N. J., Werner, F., Schwartz, M. J., et al. (2022).
478 The Hunga Tonga-Hunga Ha’apai hydration of the stratosphere. *Geophysical Research Letters*,
479 49(13). <https://doi.org/10.1029/2022gl099381>

480

481 Murphy, D. M., & Koop, T. (2005). Review of the vapour pressures of ice and supercooled water
482 for atmospheric applications. *Quarterly Journal of the Royal Meteorological Society*, 131(608),
483 1539–1565. <https://doi.org/10.1256/qj.04.94>

484

485 Peterson, D. A., Hyer, E. J., Campbell, J. R., Fromm, M. D., Van, T., Bennese, C., & Berman,
486 M. (2019). Quantifying the impact of intense pyroconvection on stratospheric aerosol loading.
487 AGU Fall Meeting Abstracts, 2019, GC11F-1150.

488

489 Proud, S. R., Prata, A. T., & Schmauß, S. (2022). The January 2022 eruption of Hunga Tonga-
490 Hunga Ha’apai volcano reached the mesosphere. *Science*, 378(6619), 554–557.
491 <https://doi.org/10.1126/science.abo4076>

492

493 Robock, A. (2000). Volcanic eruptions and climate. *Reviews of Geophysics*, 38(2), 191–219.
494 <https://doi.org/10.1029/1998rg000054>

495

496 Gelaro, R., McCarty, W., Suárez, M. J., Todling, R., Molod, A., Takacs, L., et al. (2017). The
497 Modern-Era Retrospective Analysis for Research and Applications, Version 2 (MERRA-2).
498 *Journal of Climate*, 30(14), 5419–5454. <https://doi.org/10.1175/jcli-d-16-0758.1>

499

500 Sellitto, P., Podglajen, A., Belhadji, R., Boichu, M., Carboni, E., Cuesta, J., et al. (2022). The
501 unexpected radiative impact of the Hunga Tonga eruption of 15th January 2022.
502 Communications Earth & Environment, 3(1). <https://doi.org/10.1038/s43247-022-00618-z>
503

504 Solomon, S., Daniel, J. S., Neely, R. R., Vernier, J. -p., Dutton, E. G., & Thomason, L. W.
505 (2011). The persistently variable “Background” stratospheric aerosol layer and global climate
506 change. *Science*, 333(6044), 866–870. <https://doi.org/10.1126/science.1206027>
507

508 Solomon, S., Portmann, R. W., Garcia, R. R., Thomason, L. W., Poole, L. R., & McCormick, M.
509 P. (1996). The role of aerosol variations in anthropogenic ozone depletion at northern
510 midlatitudes. *Journal of Geophysical Research Atmospheres*, 101(D3), 6713–6727.
511 <https://doi.org/10.1029/95jd03353>
512

513 Taha, G., Loughman, R., Colarco, P. R., Zhu, T., Thomason, L. W., & Jaross, G. (2022).
514 Tracking the 2022 Hunga Tonga-Hunga Ha’apai aerosol cloud in the Upper and Middle
515 stratosphere using Space-Based observations. *Geophysical Research Letters*, 49(19).
516 <https://doi.org/10.1029/2022gl100091>
517

518 Titos, G., Cazorla, A., Zieger, P., Andrews, E., Lyamani, H., Granados-Muñoz, M. J., et al.
519 (2016). Effect of hygroscopic growth on the aerosol light-scattering coefficient: A review of
520 measurements, techniques and error sources. *Atmospheric Environment*, 141, 494–507.
521 <https://doi.org/10.1016/j.atmosenv.2016.07.021>
522

523 Vernier, J. P., et al. (2009), Tropical stratospheric aerosol layer from CALIPSO lidar
524 observations, *J. Geophys. Res.*, 114, D00H10, doi:[10.1029/2009JD011946](https://doi.org/10.1029/2009JD011946).
525

526 Vernier, J. -p., Thomason, L. W., Pommereau, J. -p., Bourassa, A., Pelon, J., Garnier, A., et al.
527 (2011). Major influence of tropical volcanic eruptions on the stratospheric aerosol layer during
528 the last decade. *Geophysical Research Letters*, 38(12), n/a.
529 <https://doi.org/10.1029/2011gl047563>
530

531 Vernier, J.-P., Aubry, T. J., Timmreck, C., Schmidt, A., Clarisse, L., Prata, F., et al. (2024). The
532 2019 Raikoke eruption as a testbed used by the Volcano Response group for rapid assessment
533 of volcanic atmospheric impacts. *Atmospheric Chemistry and Physics*, 24(10), 5765–5782.
534 <https://doi.org/10.5194/acp-24-5765-2024>
535

536 Zhu, Y., Bardeen, C. G., Tilmes, S., Mills, M. J., Wang, X., Harvey, V. L., et al. (2022).
537 Perturbations in stratospheric aerosol evolution due to the water-rich plume of the 2022 Hunga-
538 Tonga eruption. *Communications Earth & Environment*, 3(1). <https://doi.org/10.1038/s43247-022-00580-w>
539
540
541
542

543

544

545

546